International Journal for Housing Science and Its Applications
Publish August 6, 2025. Volume 46, Issue 3 Pages 5537-5548

https://doi.org/10.70517/ijhsa463478

Study on the distribution of structural residual bearing capacity during the demolition process of Qingshuihe Bridge based on numerical simulation analysis

Changzhu Wang[1], Jixiang Chai[1], Hongtu Xu[1] and Zhiquan Liu[2,*]
[1] CCCC Third Highway Engineering CO., LTD., Beijing, 050000, China
[2] Bridgee Engineering Consulting of Shanghai, Shanghai, 200084, China
Corresponding authors: (e-mail: liuzhiquan2005@126.com).

Abstract With the increase of traffic flow, the road carrying level needs to be improved, more and more bridges need to be demolished and rebuilt. The primary principle of bridge demolition is safety first, but collapse accidents caused by improper construction occur from time to time. This paper takes Qingshuihe Bridge as the research object, and studies the distribution law of structural residual bearing capacity during bridge demolition by finite element numerical simulation method, so as to provide theoretical support for the safe demolition of bridges. Based on ABAQUS finite element software to establish the bridge model, using explicit finite element analysis method, the structure along the z-axis equally spaced division of 30 free slices, analyzed the distribution of internal forces and residual bearing capacity of the bridge structure under different demolition time. The study shows that: with the increase of demolition time, the maximum value of internal force in Fx direction reaches 3260kN, which occurs at the number of slices 15; the internal force in Fy direction shows a symmetric structure about the number of slices 15, with the maximum value of 8.83×104kN; the residual bearing capacity of the structure decreases from the initial 194896kN to the 144676kN in 240min, which is the rule of change of the double-exponential decay function. By comparing the tests of specimens FCD-1, FCD-2 and FCD-3 with the finite element simulation, the model errors were 9.2%, 4.3% and 5.2% respectively, which verified the accuracy of the model. This study provides a reference basis for the structural safety control during the demolition process of similar bridges such as the Clearwater River Bridge.

Index Terms Finite element analysis, Bridge demolition, Residual bearing capacity, Internal force distribution, Numerical simulation, Structural safety

I. Introduction

In the stage of high-quality development focusing on economic construction, the construction of transportation infrastructure is developing rapidly, and with the increasing traffic flow, the road carrying level needs to be improved, and the same is true for bridges as an important part of the transportation network [1], [2]. More and more bridges need to be demolished based on several factors, one is the design problem of bridges in earlier years, the previous design passing load may not be able to meet today's traffic demand [3]. Secondly, in the earlier years, the management of road construction is not standardized and strict, illegal subcontracting, subcontracting, barbaric construction, jerry-building phenomenon is common, resulting in a large number of diseases of some bridges within their design period of passage, such as cracking of the bottom plate and web, loss of prestressing, broken expansion joints, cracking of piers and pile defects, etc. [4]-[7]. The continuous development and deterioration of the disease will lead to the bridge durability and traffic safety reduction, so it is necessary to use the bridge reinforcement to deal with, part of the serious disease or reinforcement significance of the bridge needs to be demolished and rebuilt [8]-[10]. Third, some of the early construction of the bridge beam affects the local urban planning, so it needs to be demolished, which also accounts for a large part of the number of bridges demolished. Fourth, due to the improper use of the bridge caused by the bridge safety problems, the bridge can be normal passage to set up the beam counting the use of the life of the premise is the normal use and normal maintenance, overloaded vehicle traffic and the lack of regular maintenance of the bridge will lead to shorten the service life of the bridge, if necessary, need to be demolished and rebuilt [11]. The first principle of bridge demolition is safety first, however, in recent years, due to improper bridge demolition construction triggered by structural collapse accidents are endless [12]. Therefore, the study of structural mechanics of bridge demolition process is an important basis for realizing the safe demolition of bridges.

The service life of the Qingshui River bridge is more than 40 years, the structure is aging seriously, the bridge bearing capacity decreases, and at the same time, it needs to be dismantled under the demand of traffic planning. However, due to the complex traffic in the location of the bridge, its demolition needs to take into account the deformation and fluctuation of the bridge structure during the demolition process to reduce and prevent accidents from occurring. Based on this, it is important to explore the distribution of the remaining structural load carrying capacity during the demolition process to provide a reference for safe demolition programs.

In the stage of high-quality development with a focus on economic construction, the construction of transportation infrastructure has developed rapidly, and as traffic flows continue to increase, the level of roadway capacity needs to be improved, and the same is true for bridges as an important part of the transportation network. More and more bridges need to be dismantled due to the following factors: firstly, the design of bridges in earlier years may not be able to meet today's traffic demand with the previous design load. Secondly, in the earlier years, the road construction management is not standardized and strict, illegal subcontracting, subcontracting, brutal construction, jerry-building phenomenon is common, resulting in a large number of bridges in their design period of time to appear a lot of disease, such as the bottom plate, web cracking, loss of prestressing, expansion joints broken, pier cracking and piling defects and so on. The continuous development of disease deterioration will lead to bridge durability and safety reduction, so must be used to strengthen the bridge to deal with the way, part of the disease is serious or reinforce the significance of the bridge needs to be demolished and rebuilt. Third, some of the early construction of the bridge affects the local urban planning, so it needs to be demolished, which also accounts for a large part of the number of bridge demolition. Fourth, due to the improper use of bridges caused by the bridge safety problems, bridges can be normal passage to the design life of the premise of normal use and normal maintenance, overloaded vehicles and the lack of regular maintenance of bridges will lead to shorten the service life of bridges, if necessary, need to be dismantled and rebuilt. The first principle of bridge demolition is safety first, however, in recent years, due to improper bridge demolition construction triggered by structural collapse accidents are endless. Therefore, the study of structural mechanics of bridge demolition process is an important basis for realizing the safe demolition of bridges. In this paper, the Qingshuihe Bridge is selected as the research object, the bridge service life of more than 40 years, the structure of the aging is serious, the bridge bearing capacity decline, and at the same time in the traffic planning needs to be dismantled. However, because the bridge is located in a complex traffic location, its demolition needs to take into account the deformation and fluctuation of the bridge structure during the demolition process to reduce and prevent accidents. Based on this, this paper adopts the finite element analysis method to numerically simulate the structural mechanical behavior of Qingshuihe Bridge during the demolition process, focusing on the distribution of the internal force and the change rule of the residual bearing capacity of the bridge structure under different demolition time nodes. In the study, first of all, establish the refined finite element model of Qingshuihe Bridge, divide the bridge structure along the z-axis at equal intervals into 30 free slices, extract the internal force and bending moment of the structure in x, y and z axes after different dismantling time and analyze them respectively. Then, the accuracy of the model is verified by comparing the model calculation results with the test data, and the influence of parameters such as the height of the concrete roof slab on the residual bearing capacity of the bridge deck slab is further analyzed.

II. Theories related to finite element analysis methods

II. A. Fundamentals

Explicit finite element analysis method and implicit finite element analysis method are two commonly used finite element analysis methods during finite element simulation [13]. The basic principles of the explicit analysis method are described below.

From the basic principles of D'Alembert dynamics, the dynamical equilibrium equations of the system can be obtained:

$$m\ddot{u} + c\dot{u} + ku = r(t) \tag{1}$$

In Eq. (1), $\ddot{u}, \dot{u}$ and u denote the acceleration, velocity and displacement of the system, respectively, and $r(t)$ denotes the external load.

If the solution is carried out by the finite element method, written in matrix form, the matrix form of the structural dynamics equations of the system is:

$$M\ddot{U} + C\dot{U} + KU = R \tag{2}$$

where M, C and K denote the mass, damping, and stiffness matrices of the system, respectively. $\ddot{U}, \dot{U}$ and U are the acceleration, velocity, and displacement matrices of the system. R is the external load vector.

Assuming that the displacement and velocity-acceleration vectors of the system at the initial moment $t = 0$ are known, and that the solution of Equation (2) for the moments 0 to T is solved by dividing the full duration of time T

into n equal time segments Δt, the velocities and accelerations at the moments t can be expressed by the following equations:

$$\ddot{U}_t = \frac{1}{\Delta t^2}(U_{t+\Delta t} - 2U_t + U_{t-\Delta t}) \tag{3}$$

$$\dot{U}_t = \frac{1}{2\Delta t}(U_{t+\Delta t} - U_{t-\Delta t}) \tag{4}$$

Substituting (3) and (4) into the structural dynamics equations of the system at the moment of t is obtained:

$$\hat{R}_{t+\Delta t} = R_{t+\Delta t} - \left(K - \frac{2M}{\Delta t^2}\right)U_t - \left(\frac{M}{\Delta t^2} - \frac{C}{2\Delta t}\right)U_{t-\Delta t} \tag{5}$$

According to the above equation, $U_{t+\Delta t}$ can be found, and since the solution for the displacement of the system at the moment $t+\Delta t$ is obtained by using the equilibrium conditions of the system at the moment t, this integration process and method is known as the explicit integration method [14].

II. B.LS-DYNA based finite element crash analysis method

II. B. 1) Type of unit

LS-DYNA program provides a variety of different cell types, in the face of different structures, the choice of the appropriate cell type can significantly improve the accuracy of the numerical simulation model and its computational efficiency, and the problem of non-convergence of the calculation results can also be avoided to a certain extent by choosing the appropriate cell. , beam unit, shell unit.

II. B. 2) Concrete material model

There are three main types of concrete structure models in common use:

(1) Concrete damage model (MAT_72R3)

Concrete damage model * MAT_CONCRETE_DAMAGE_REL3 model describes its mechanical behavior through the initial yield surface, the maximum strength failure surface and the residual strength surface of the three strength surfaces, the strength surface of the unified expression is:

$$\Delta\sigma = \sqrt{3J_2} = f(p, J_2, J_3) \tag{6}$$

where $\Delta\sigma$ and p are the principal stress differential and hydrostatic pressure, respectively. where $f(p, J_2, J_3) = \Delta\sigma^c \times r'$, $\Delta\sigma$ and r' are the compressed meridional and normalized willam- Warke partial plane model. Namely:

$$r' = \frac{2(1-\psi^2)\cos\theta + (2\psi-1)\sqrt{4(1-\psi^2)\cos^2\theta + 5\psi^2 - 4\psi}}{4(1-\psi^2)\cos^2\theta + (1-2\psi)^2} \tag{7}$$

It can be seen that the value of r' depends on ψ and θ. When θ is 60°, $r' = 1$, which is expressed as a function of the compression meridian of the three strength surfaces in the uniaxial state-of-pressure concrete damage model is expressed as:

Initial yield surface:

$$\Delta\sigma_y^c = a_{0y} + \frac{p}{a_{1y} + a_{2y}p} \tag{8}$$

Maximum strength failure surface:

$$\Delta\sigma_m^c = a_0 + \frac{p}{a_1 + a_2 p} \tag{9}$$

Residual strength surfaces:

$$\Delta\sigma_r^c = \frac{p}{a_{1f} + a_{2f}p} \tag{10}$$

where $a_{0y}, a_{1y}, a_{2y}, a_0, a_1, a_2, a_{1f}, a_{2f}$ is the performance parameter of the material. The current stress state of the material can be calculated by the difference method based on the failure surface.

(2) JHC model (MAT_111)

The strength of the JHC model after yielding is obtained from the initial failure surface after discounting, and its initial failure surface is:

$$\sigma^* = [A + BP^{*N}] \times (1 + C\ln\varepsilon^*) \text{ when } \sigma^* \le SMAX$$
$$\sigma^* = SMAX \text{ when } \sigma^* > SMAX \tag{11}$$

where σ^* represents the normalized material strength, $\sigma^* = \sigma / f_c$, where σ is the actual equivalent stress. P^* is the normalized hydrostatic pressure, $P^* = P / f_c$, where P is the actual hydrostatic pressure. $\dot{\varepsilon}^*$ is the reference strain rate, $\dot{\varepsilon}^* = \dot{\varepsilon} / \dot{\varepsilon}_0$, where ε is the actual strain rate and $\dot{\varepsilon}_0$ is the reference strain rate. $SMAX$ is the highest strength value of the material, A, B, N and C are material constants.

The yield surface equation after failure of the JHC model is defined in the following equation:

$$\sigma^* = \left[A(1-D) + BP^{*N} \right](1 + C \ln \dot{\varepsilon}^*) \tag{12}$$

D is the damage factor of the material, which can be expressed by the following equation:

$$D = \sum \left[(\Delta\varepsilon_P + \Delta\mu_P) / \varepsilon_P^f + \mu_P^f \right] \tag{13}$$

Where $\Delta\varepsilon_p$ is the equivalent plastic strain of the material, and $\Delta\mu_p$ denotes the incremental plastic volume strain of the material. The expressions ε_p^f and μ_p^f are the plastic strain and plastic volume strain under normal pressure, respectively:

$$\varepsilon_p^f + \mu_p^f = D_1 (P^* + T^*)^{D_2} \tag{14}$$

where D_1, D_2 are material parameters. $T^* = T / f_c$ is the uniaxial tensile strength of the material after normalization of the compressive strength.

II. B. 3) Reinforcing steel material model

Reinforcing steel materials are generally simulated using the bilinear elasto-plastic model *MAT_PLASTIC_KINEMATIC (MAT_3). The elasto-plastic hardening model is shown in Fig. 1, which describes the following hardening of the material and the various isotropic hardening properties during cyclic loading. The strain rate effect of the material under impact loading can be considered by the Cower-Symonds model.

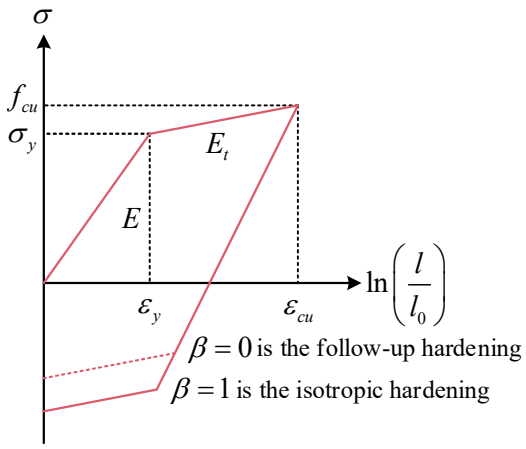

Figure 1: Elastoplastic hardening model

$$\sigma_y = \left[1 + \left(\frac{\dot{\varepsilon}}{C} \right)^{1/P} \right](\sigma_0 + \beta E_p \varepsilon_{eff}^p) \tag{15}$$

where C and P are the strain rate parameters of the material and ε is the strain rate of the steel bar under impact. τ_0 is the yield stress of the steel bar. β and E_p are the hardening parameter and plastic strengthening modulus of the rebar, respectively. ε_{eff}^p is the effective plastic strain of the rebar.

II. B. 4) Hourglass model

In the calculation of complex nonlinear problems with finite element analysis, in which the integral calculation of the unit takes up most of the time and computational resources, in order to improve the computational efficiency, LS-DYNA unit algorithm is generally used in the single-point reduced Gaussian integral algorithm, relative to the full integral algorithm, single-point integral significantly reduces the number of calculations, saves the computation time and meets the requirements of the structural analysis of large deformations. In order to ensure the accuracy of the calculation, it is necessary to control the hourglass energy, generally the hourglass is within 10% of the total energy,

then the results can be considered relatively accurate. When the hourglass energy is too large, it can often be solved by optimizing the grid size, adopting the full-integration unit, and adopting a reasonable hourglass control mode.

II. B. 5) Contact Collision Algorithm

When performing finite element numerical analysis of the impact collision process, the simulation of the contact behavior between the impactor and the structure as well as the various components of the structure is crucial to the accuracy of the numerical simulation results. The LS-DYNA finite element program, which has a powerful ability to analyze contact nonlinear problems, has three main methods for dealing with the collision and sliding contact problems at the contact interface, namely, the penalty function algorithm, the dynamic constraint method, and the distribution parameter method.

III. Dynamic characterization of the Clearwater River bridge

III. A. Basic Theory of Structural Dynamic Characterization

Engineering structures can be regarded as dynamic systems composed of stiffness, mass and damping matrices, and modal analysis is usually chosen to study the structural dynamic characteristics, i.e., the structural self-oscillation characteristics, including the structure's vibration mode and period. Among them, the modes of the structure are its inherent characteristics, which are only related to the type of material chosen for the structure itself, the cross-section size of the structural members and the plan layout of the structure, and the intrinsic frequency and vibration mode of the structure can be obtained through modal analysis, which is an important link for the dynamic design and damage detection of the structure [15]. In addition, the structural dynamic characteristic data obtained through modal analysis can be applied to other analyses, such as response spectrum analysis, transient dynamic analysis and dynamic time course analysis.

The essence of modal analysis is to calculate the eigenvalues and eigenvectors of the structural vibration equations consisting of mass and stiffness, and the vibration equations of a multi-degree-of-freedom structural system are as follows:

$$[M]\{\ddot{u}\}+[C]\{\dot{u}\}+[K]\{u\}=\{P(t)\} \tag{16}$$

where $\{\ddot{u}\},\{\dot{u}\},\{u\}$ are the acceleration, velocity, and displacement vectors, respectively. $[M]$ is the mass matrix of the structure. $[C]$ is the damping matrix of the structure. $[K]$ is the stiffness matrix of the structure. $\{P(t)\}$ is the external load matrix. All the above matrices are n-dimensional matrices and n is equal to the degrees of freedom of the structure. Therefore, the free vibration equation of the structure in the undamped state can be introduced as:

$$[M]\{\ddot{u}\}+[K]\{u\}=0 \tag{17}$$

If this vibration is a simple harmonic vibration, the equation can be transformed into:

$$\{u\}=\{\hat{u}\}sin(\omega t+\theta) \tag{18}$$

where $\{\hat{u}\}$ denotes the structure amplitude. ω denotes the vibration circular frequency and θ denotes the phase angle, then the structure free vibration equation can be transformed into:

$$([K]-\omega^2[M])\{\hat{u}\}=0 \tag{19}$$

When and only when:

$$([K]-\omega^2[M])=0 \tag{20}$$

It is when the structure is guaranteed to do free vibration with finite amplitude. The equation is called the frequency equation of the structure, and when the structure has n degrees of freedom, arranging the n solutions of the frequency equation in sequence gives the circular frequency vector $\{\omega\}$ of the structure, i.e.:

$$\{\omega\}=\{\omega_1\omega_2\omega_3\ldots\omega_n\}^{\mathrm{T}} \tag{21}$$

After obtaining the vibration frequency, the vibration equation can be written as:

$$\bar{E}_n\{\hat{u}\}=0 \tag{22}$$

$$\bar{E}_n=[K]-\omega^2[M] \tag{23}$$

From Eq. It can be seen that $\bar{E}^n$ takes values related to the vibration frequency, so the vibration pattern of the structure varies with the vibration frequency, and let the first element of the displacement vector be a unit amplitude, then the n vibration patterns Φ_i form Φ, i.e., the vibration pattern matrix:

$$\Phi=[\Phi_1\Phi_2\Phi_3\ldots\Phi_n] \tag{24}$$

III. B. Overview of bridges

In this paper, the Clearwater River Bridge is studied, the main bridge span combination is 161 m+720 m+161 m. The bridge adopts a partially ground-anchored structural system of "girder-tower separation, girder platform consolidation", the main girder is consolidated with ground-anchored abutment, the main girder is separated from the cable-stayed tower, and the cable-stayed tower is equipped with a No. 0 cable-stayed cable as a vertical support, and two pairs of transverse bearings are set up, and a structure of "main girder central axle-free joint+expansion joint" is set up in the middle of the main span to link the two halves of cable-stayed bridge on the south and north banks. In the middle of the main span, the structure of "no axial joint + expansion joint in the center of the main girder" is set up to connect the two halves of the cable-stayed bridge on the south and north banks into one. The main bridge cable-stayed towers are H-type towers in the cross-bridge direction, which are made of C55 concrete, with a tower height of 192.4 m. There are 4×26 pairs of cables, each cable is composed of zinc-aluminum-alloy coated parallel steel wires with an ultimate tensile strength of 1,860 MPa, which are uniformly distributed according to the fan shape, and the standard distance between the steel girders of the main span and the side-span PC girders is 16 m. The distance between the PC girders of the side-span and the side-span is 8 m. The distance between the anchored abutment and the side-span is 3.5 m. The distance between the cable-stays is 3.5 m. The standard cable spacing of ground-anchored abutment section is 3.5m.

In order to reduce the weight of the main span and enhance the bending capacity of the main girder, the main girder portion of the center span adopts separated double side box section girders and orthogonal anisotropic deck slabs. The two side spans adopt PC side main girders with uniform appearance with the steel box girders in the middle span. The steel main girder members are all made of Q420 steel, the side spans are made of C50 concrete, and the compression weight section of the side spans is made of C55 concrete. The main bridge of Qingshuihe Bridge is a monolithic section, the standard section of box girder of the main bridge is 31.6m, the height from the top edge of the steel box girder top plate to the top edge of the bottom plate is 3.8m, the standard width of the bridge deck is 26m, and the layout is four lanes in both directions and the shoulders of left and right are 2.8m each.

According to the structural characteristics of the bridge, natural conditions of the bridge, transportation equipment and lifting capacity, erection period and many other factors, the steel main girder can be divided into 24 steel girder sections from the steel-hybrid bonding surface to the center section of the steel girder, such as steel-hybrid bonding section, steel main girder section, and closing section, etc. The bridge is a symmetrical structure, so the whole bridge has a total of 48 girder sections. The cross-section parameters of top plate and web plate of each side box girder section are the same, and only change in the area of bottom plate of box girder. According to the different thickness of the bottom plate, the steel main girder sections are divided into 8 categories.

III. C. Finite element analysis model

According to the specific structure of steel main girder section, 8 types of steel main girder sections are drawn. Finally, through the cross-section characteristic calculation function of Midas/Civil software (SPC cross-section manager), the drawn steel main girder cross-section was calculated by cross-section characteristic calculation, imported into Midas Civil, and assigned the cross-section according to the corresponding unit to generate the initial model of the bridge. In the modeling process, X is defined as the longitudinal direction of the bridge, Y is the transverse direction, and Z is the vertical direction. In the model building process, the real bridge was simplified appropriately, the main tower and main girder parts were modeled by girder units, and the tension-only unit was selected for the tension cable, and the program will automatically calculate the tension cable according to the elastic modulus correction formula [16]. The main girder and the tension cable, the main tower and the tension cable are all elastic links, and the rest of the constraints are handled according to the drawing layout.

IV. 4. Experimental results and analysis

IV. A. Finite Element Model Based Dynamic Characterization and Bearing Capacity Analysis

IV. A. 1) Internal Force Analysis of the Clearwater River Bridge Structure after Different Dismantling Times

In this section, the main purpose is to study the force behavior of the structure of the Qingshuihe Bridge. Using ABAQUS finite element software for the established model, the structure is divided into 30 free slices at equal intervals along the z-axis, and the internal forces and bending moments of the structure of the Qingshuihe Bridge along the x-, y-, and z-axis are extracted and analyzed respectively after different demolition times. The variation curves of Fx internal force values under different demolition times are shown in Fig. 2. With the continuous increase of time, the value of internal force in the Fx direction at the same slice position increases gradually, in which the maximum value of internal force in the Fx direction is 3260.00 kN, and the distribution of internal force is similar in 10min, 20min and 30min, and the frequency of fluctuation of the change curve of the value of the internal force is small, and the distribution of internal force is similar in 60min, 90min and 120min, and the frequency of the change curve of the value of the value of the internal force is larger, and the maximum value occurs in all of them. The

distributions of internal forces were similar for 60min, 90min and 120min, and the fluctuations of internal force values were more frequent, with the maximum values occurring at the number of slices 16.5. The distributions of internal forces were similar for 180min and 240min, and the curves of changes in internal force values were basically symmetrical, with the maximum values occurring at the number of slices 15. The internal force on both sides is basically 0kN.

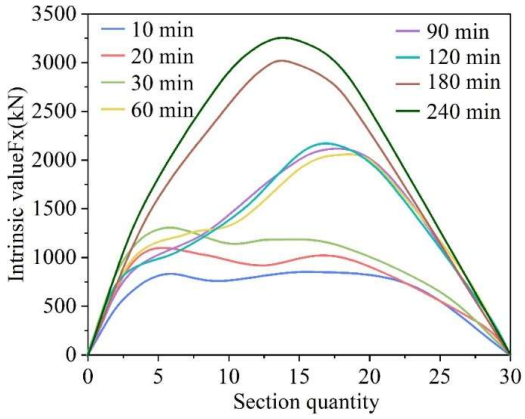

Figure 2: The change curve of the internal force value of the Fx

The change curves of Fy internal force values under different removal times are shown in Fig. 3. The change curve of Fy direction internal force of Qingshuihe Bridge shows a symmetric structure about the number of slices is 15. With the continuous increase of fire time, the absolute value of the Fy-direction internal force at the same slice position increases gradually, in which the maximum value of the Fy-direction internal force occurs at the slice number of 27, with the value of 8.83×104 kN. when the slice number is 0, 15 and 30, the value of the Fy-direction internal force is all 0 kN.

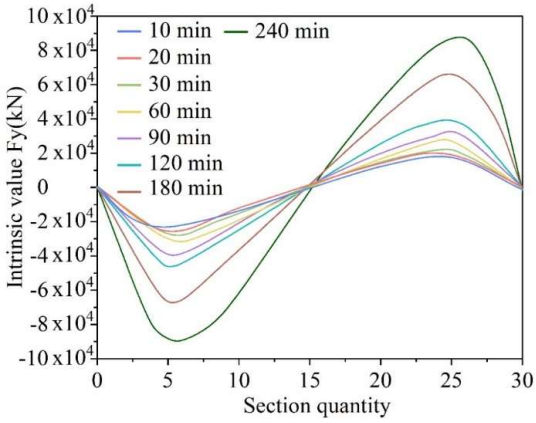

Figure 3: Different curve of the internal force value of the Fy

The change curves of Fz internal force values under different removal times are shown in Fig. 4. Because the internal force is extracted by slicing along the z-direction in the three-dimensional spatial coordinate system, the change curve of the Fz-direction of Qingshuihe Bridge is symmetric with respect to the number of slices being 15. And in different removal times, the internal force changes in Fz direction of Qingshuihe Bridge are different, but the fluctuations of the changes are small.

The variation curves of Mx bending moment values at different demolition times are shown in Fig. 5. Due to the deformation caused by concrete expansion deformation, load action and constraints together lead to the structure within the removal time of each Mx curve of bending moment first decrease and then increase, the overall along the cross-section in about the number of slices equal to 15 is symmetrically distributed, which in the tunnel on both sides of the maximum value of the bending moment, the maximum value of -2.8 × 1010kN·mm, plus and minus sign indicates the bending moment of the direction.

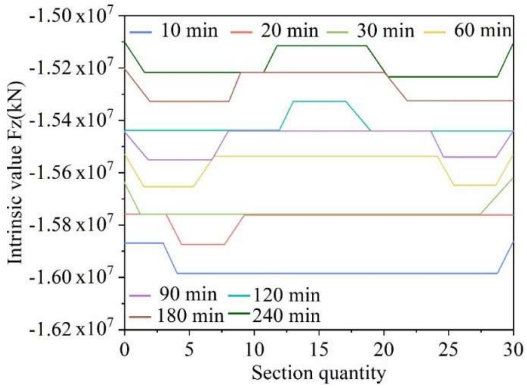

Figure 4: The change curve of the internal force value of the Fz

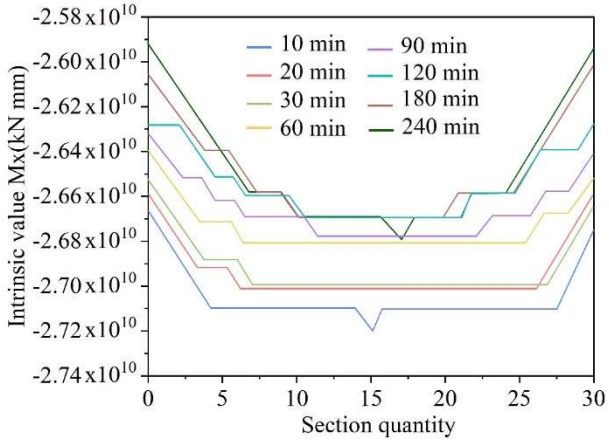

Figure 5: The change curve of the internal force value of the Mx

The change curves of My bending moment values at different dismantling times are shown in Fig. 6. The distribution of bending moments at 10min, 20min and 30min are similar, and the frequency of fluctuation of the change curve of the bending moment value is small. 60min, 90min and 120min have similar bending moment distributions and the frequency of fluctuation of the curve of the change of the bending moment value is larger. 180min and 240min have similar bending moment distributions, and the frequency of fluctuation of the curve of the change of bending moment is the fastest. The bending moment distribution is similar for 180min and 240min, and the frequency of fluctuation of the growth curve of bending moment change is the fastest. The maximum value of the bending moment is 2.6×107kN·mm on one side, and the plus and minus signs indicate the direction of the bending moment.

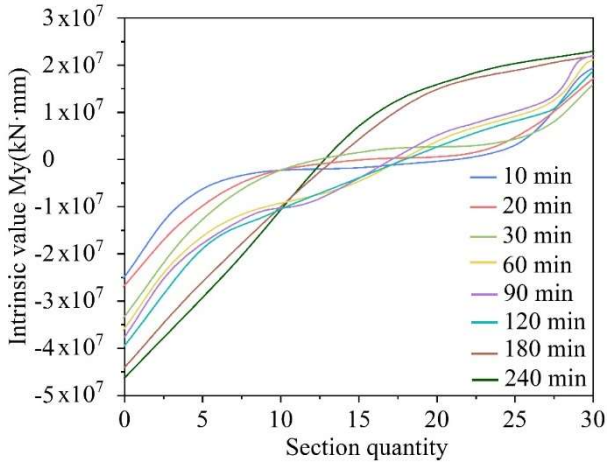

Figure 6: The change curve of the internal force value of the My

The change curves of Mz bending moment values under different demolition times are shown in Fig. 7. The change curve of Mz bending moment value in the direction of Qingshuihe Bridge increases and then decreases as a whole, and the maximum bending moment value occurs after 240 min of demolition, with a value of 3.12×107kN·mm, and the plus and minus signs represent the direction of the bending moment at the location. And with the continuous increase of time, the deformation caused by the expansion deformation of concrete, load action and constraint together lead to the longer removal time at the same slice position, the larger the value of the Mz direction bending moment.

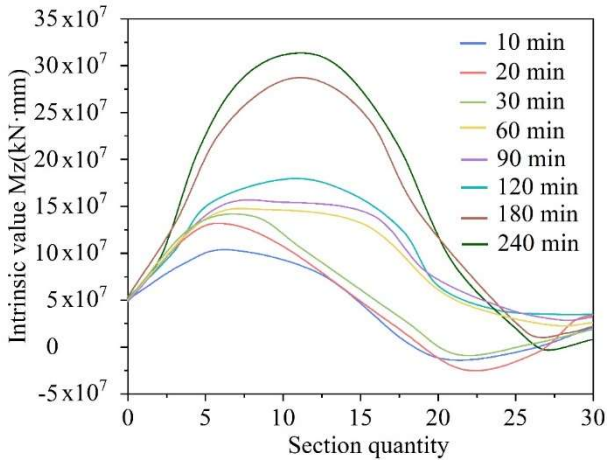

Figure 7: The change curve of the internal force value of the Mz

IV. A. 2) Residual Capacity Analysis of Clearwater River Bridge Structures

The residual bearing capacity of the Clearwater River bridge structure at different demolition times is shown in Table 1.

Table 1: The residual capacity of the water river bridge structure under different removal time

Time (min)	0	10	20	30	60	90	120	180	240
Residual bearing capacity (kN)	194896	186112	180117	170866	166227	159865	156585	152211	144676

Fitted according to the table, the fitted relationship graph of the residual bearing capacity with the change of demolition time is shown in Fig. 8. The residual bearing capacity of the structure of the Clearwater River bridge decreases gradually with the increase of the demolition time, and the overall change rule of double-exponential decay function is shown.

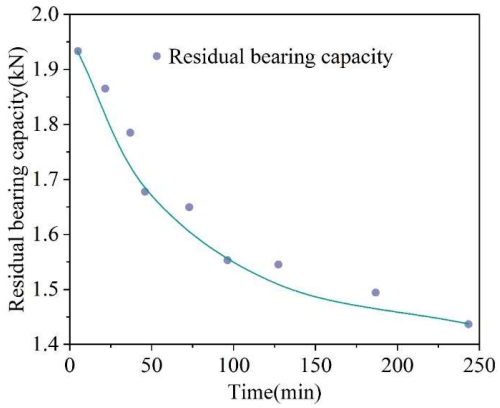

Figure 8: Changes of highway tunnels with depth under different fire times

IV. B. Model Performance Tests

IV. B. 1) Finite element model validation

The modeling analysis of the combined bridge deck specimens was carried out by ABAQUS, and the residual bearing capacity of specimens FCD-1, FCD-2, and FCD-3 were obtained to be 435.6 kN, 344.9 kN, and 316.8 kN, respectively.The load-slip curves are shown in Fig. 9. The slopes of the two curves are basically the same at the beginning of loading. The load-slip curves of specimens FCD-1 and FCD-2 after yielding were not obtained because their steel base plates were unloaded after reaching the yield strength during static loading. By comparing the finite element results of specimen FCD-3 with the experimental results, it was found that the changes in the linear stage and the yielding stage of the two were basically the same, and the maximum deflections of the two were 31.8 mm and 34.9 mm, respectively, with an error of 6.7%. The residual load capacity comparison is shown in Fig. 10, and the errors of the three are 9.2%, 4.3%, and 5.2%, respectively, which indicates that the finite element model has good accuracy. The load-displacement curves of the finite element results in the figure show large fluctuations in the late loading stage, which may be caused by the fast loading speed.

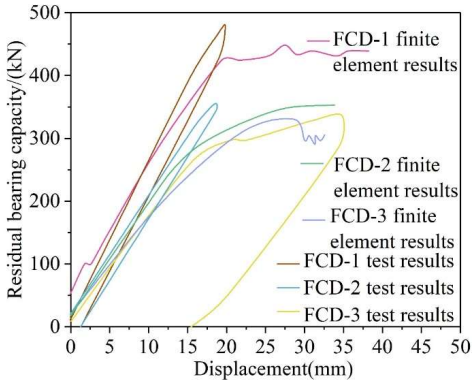

Figure 9: Load-slip curve

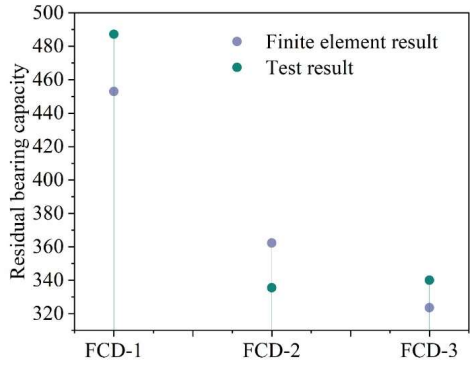

Figure 10: The residual bearing capacity is compared

IV. B. 2) Parametric analysis of the height of concrete roof slabs

In this section, the effect of the height of the concrete top slab on the residual bearing capacity of the bridge deck slab is analyzed by taking specimen FCD-3 as an example. The variation of concrete roof slab height is shown in Fig. 11 (Fig. a shows the residual bearing capacity under different concrete roof slab heights, and Fig. b shows the fitting curve of concrete roof slab height and residual bearing capacity). In order to study the effect of the variation of concrete roof height on the residual bearing capacity of specimen FCD-3, in this section, the concrete roof height was taken as 145mm, 175mm, 205mm, 235mm, respectively, and the corresponding residual bearing capacity of the specimen was obtained as 452.3kN, 566.1kN, 656kN, 765kN through the analysis and calculation of ABAQUS, as shown in Fig. (a). shown. With the increase of the height of the concrete roof slab, the residual bearing capacity of the specimen under the same displacement in the linear stage increases, which indicates that the increase of the height of the roof slab can effectively improve the stiffness of the specimen. The corresponding fitting curves were obtained by fitting different concrete roof heights to the residual load capacity, as shown in Fig. (b), the residual load capacity of the specimen increases linearly with the increase of the roof height.

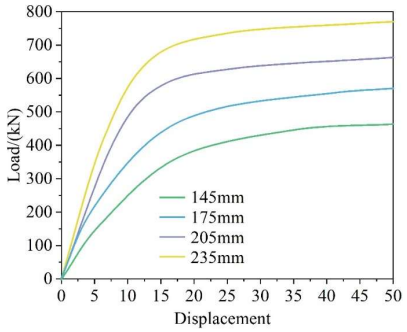

(a) The residual capacity of different concrete roof is high

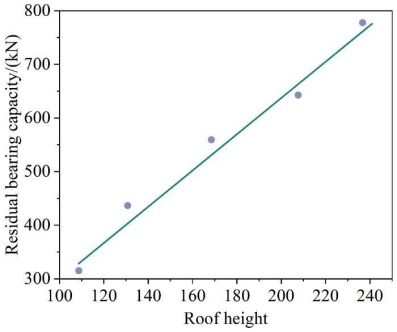

(b) The height of the concrete roof and the fitting curve of the residual bearing capacity

Figure 11: The concrete roof is highly varied

V. Conclusion

In this paper, the distribution law of structural residual bearing capacity in the demolition process of Qingshuihe Bridge is investigated by finite element numerical simulation method, and the following conclusions are drawn:

1. With the continuous increase of dismantling time, the distribution of the internal force of the bridge structure shows regular changes. the maximum value of the internal force in the Fx direction is 3260kN, which occurs at the number of slices 15; the internal force in the Fy direction shows a symmetric structure about the number of slices 15, with the maximum value of 8.83×104kN, which occurs at the number of slices 27; the maximum value of the bending moment in the Mz direction is 3.12×107kN -mm, which appeared after 240 min of demolition.

2. The residual bearing capacity of the Clearwater River bridge structure decreases gradually with the increase of demolition time, from 194896kN in the initial state to 144676kN after 240min of demolition, and the overall rule of change of double-exponential decay function. This shows that the structural safety reserve gradually decreases during the demolition process, and the monitoring and control should be strengthened in the later stage of demolition.

3. Comparing the specimen test and finite element simulation, it is found that the error between the finite element results of FCD-3 and the test results in terms of maximum deflection is 6.7%, and the errors of the residual bearing capacity of the three groups of specimens are 9.2%, 4.3s% and 5.2%, which verifies the accuracy and reliability of the model.

4. The height of the concrete roof slab has a significant effect on the residual bearing capacity of the bridge deck slab. When the height of concrete top slab was 145mm, 175mm, 205mm and 235mm, the residual bearing capacity of specimen FCD-3 was 452.3kN, 566.1kN, 656kN and 765kN, respectively, which showed a linear growth trend. This indicates that in the process of bridge reinforcement or reconstruction, increasing the height of the concrete roof slab appropriately can effectively improve the structural bearing capacity.

Funding

This work was supported by Research on Key Technologies for Uninterrupted Navigation, Cross Canal Multi porous Continuous Beam Demolition, and Tied Arch Bridge Reconstruction (SGJLGSKY-2024-01).

References

[1] Spinella, N., & Messina, D. (2023). Load-bearing capacity of Gerber saddles in existing bridge girders by different levels of numerical analysis. Structural Concrete, 24(1), 211-226.

[2] Bucsky, P., & Juhász, M. (2022). Long-term evidence on induced traffic: A case study on the relationship between road traffic and capacity of Budapest bridges. Transportation research part A: policy and practice, 157, 244-257.

[3] Murphy, B., Locum, J., Belser, M., Bhegani, K., & Yarnold, M. (2018). Dead load evaluation through truss bridge deconstruction monitoring. Journal of Bridge Engineering, 23(1), 04017115.

[4] Yao, Y., Fu, Z., Ji, B., Wang, Q., & Gong, Y. (2024, October). Stress characteristics and cracking mechanism of web-to-stiffener weld in steel plate girder bridges under bending-shear action. In Structures (Vol. 68, p. 107088). Elsevier.

[5] Chen, T. T. (2017). Factors in bridge failure, inspection, and maintenance. Journal of Performance of Constructed Facilities, 31(5), 04017070.

[6] Bonopera, M., Chang, K. C., & Lee, Z. K. (2020). State-of-the-art review on determining prestress losses in prestressed concrete girders. Applied Sciences, 10(20), 7257.

[7] Guo, T., Huang, L., Liu, J., & Zou, Y. (2018). Damage mechanism of control springs in modular expansion joints of long-span bridges. Journal of Bridge Engineering, 23(7), 04018038.

[8] Wei, X., & Peng, D. (2021, November). Disease Analysis And Treatment of A Prestressed Concrete Continuous Curved Beam Bridge. In 2021 4th International Symposium on Traffic Transportation and Civil Architecture (ISTTCA) (pp. 486-490). IEEE.

[9] Li, S., Ou, J., Wang, J., Gao, X., & Yang, C. (2019). Level 2 safety evaluation of concrete-filled steel tubular arch bridges incorporating structural health monitoring and inspection information based on China bridge standards. Structural Control and Health Monitoring, 26(3), e2303.
[10] Fu, M., Liang, Y., Feng, Q., Wu, B., & Tang, G. (2022). Research on the application of multi-source data analysis for bridge safety monitoring in the reconstruction and demolition process. Buildings, 12(8), 1195.
[11] Han, W., Yuan, Y., Chen, X., Xie, Q., Gao, G., & Zhang, J. (2018). Safety assessment of continuous beam bridges under overloaded customized transport vehicle load. Journal of Bridge Engineering, 23(6), 04018030.
[12] Tang, D., & Huang, M. (2024). The sustainable development of bridges in China: Collapse cause analysis, existing management dilemmas and potential solutions. Buildings, 14(2), 419.
[13] Wenjuan Li,Fuzheng Gao & Jintao Cui. (2025). Error analysis of implicit-explicit weak Galerkin finite element method for time-dependent nonlinear convection-diffusion problem. Applied Numerical Mathematics,209,232-241.
[14] Xie Cong & Wang Kun. (2021). Viscosity explicit analysis for finite element methods of time-dependent Navier–Stokes equations. Journal of Computational and Applied Mathematics,392.
[15] Xinpeng Wang,Shengxiang Huang,Chao Kang,Guanqing Li & Chenfeng Li. (2020). Integration of Wavelet Denoising and HHT Applied to the Analysis of Bridge Dynamic Characteristics. Applied Sciences,10(10).
[16] Ying Wang,Jian Xin Liu & Chong Wang. (2011). Finite Element Analysis about Dynamic Characteristics of the High-Pier and Long-Span Continuous Rigid Frame Bridge. Advanced Materials Research,1269(243-249),1876-1880.